INVITED PAPERS

Electron equilibrium and confinement in a modified Penning trap and its application to Penning fusion*

D. C. Barnes,† M. M. Schauer, and K. R. Umstadter
Los Alamos National Laboratory, Los Alamos, New Mexico 87545

L. Chacon[a] and G. Miley
Fusion Studies Laboratory, University of Illinois, Urbana, Illinois 61801

(Received 19 November 1999; accepted 14 January 2000)

The Penning fusion concept is described. Recent theoretical work on eliminating limitations on thermonuclear gain (Q) associated with ion–ion collisions is reviewed. A critical issue identified is the demonstration of the desired spherical electron configuration. Constraints on the electron distribution function are derived. A small combined trap (majority electrons), PFX-I (Penning Fusion eXperiment-Ions) has been constructed to study these issues. PFX-I is described. Two diagnostics described for electrons are destructive dumping of trapped electrons and noninvasive optical detection of impact induced fluorescence. Initial results of PFX-I operation at applied voltages V_0 up to 2 kV and magnetic fields B up to 1.14 T are described. Electron equilibrium is found to be consistent with trap filling to the space charge limit, with inventory proportional to V_0 and independent of B. Electron confinement times range from 1 to 10 ms and are determined by neutral pressure. These results are interpreted and future directions sketched. © *2000 American Institute of Physics.* [S1070-664X(00)93505-5]

I. INTRODUCTION AND BACKGROUND

A unique plasma confinement principle is being investigated. In this approach, called Penning Fusion (PF), a nonneutral electron plasma is confined in a modified Penning trap by a combination of applied magnetostatic and electrostatic fields. The electron space charge, in turn, electrostatically confines a minority, unmagnetized ion species. To apply such a system to fusion energy production, it is necessary to raise the applied voltages (producing the confining electrostatic field) to the order of 100 kV or greater. Even with such a high potential, in a practically sized system, the electron density (and to a greater degree the ion density) falls short of that required to give reasonable fusion reactivity. Thus, intrinsic to PF being an interesting concept is the idea of ion focusing, either in space or time, or some other means of enhancing ion reactivity. In this way the reactivity may be greatly enhanced over that available with the background density.

Penning Fusion is related to Inertial Electrostatic Confinement (IEC), a concept first investigated over three decades ago.[1] In IEC, a high-transparency spherical grid is placed inside a grounded spherical vessel and raised to a high negative potential relative to the vessel. Ions produced near the vessel wall are accelerated up to the several tens of kilovolts applied to the grid, and the majority of these ions pass through the grid and form a focus near the spherical center where fusion reactions occur, producing a useful flux of high-energy neutrons.

Penning Fusion attempts to address two limitations of IEC. First, in a manner similar to a concept described by Bussard and Krall,[2,3] the grid is replaced by an electron cloud, which forms a virtual cathode. In this way, ion-grid collisions and associated limitations (such as secondary electron emission from the grid and grid heating) are avoided. Second, the effects of ion–ion collisions, which limit the theoretically achievable fusion gain Q (fusion power/input power) to around unity are avoided.[4,5] Recently, work on IEC and PF has led to several suggestions for avoiding ion–ion collision effects.

A relatively old idea is the formation of multiple potential wells within the spherical system.[1] These have been inferred from recent diagnostics of IEC systems.[6,7] A second approach is based on observations from bounce-averaged Fokker–Planck calculations.[8–11] These calculations show that the self-consistent ion distribution may be well described as a two component system, one component being the radially converging beam corresponding to the injected ions, and the second a trapped Maxwellian component. Depending on parameters of ion source and sink strengths, the configuration may be dominantly beam or Maxwellian.[11] In the latter case, Q is high, since ion–ion collisions have little effect on the Maxwellian component. An optimum balance between Q and power density may then be accomplished by a proper ratio of the two components. Finally, the suggestion has been made and analyzed to replace the steady, spatial

*Paper DI 1 4 Bull. Am. Phys. Soc. **44**, 86 (1999).
†Invited speaker.
[a]Present address: Los Alamos National Laboratory, Los Alamos, New Mexico 87545.

focusing of traditional operation [called Spherically Convergent Ion Focus (SCIF)] with temporal focusing using large-amplitude collective radial ion oscillations.[12–14] In this approach [Periodically Oscillating Plasma Sphere (POPS)] there is no effect of ion–ion collisions, if the ion cloud assumes a Gaussian profile.

Many of these ion physics issues can and are being studied in IEC configurations which are intrinsically simpler and which offer relatively good diagnostic access. To make a gross oversimplification, one might assert that theory has shown that ion issues for PF are well in hand, and demonstration of a suitable electron configuration would be the basis for a PF proof-of-principle demonstration. Electron issues for PF are not easily addressed by theory alone. These issues include the reliable application of high potentials to a small system (to produce a realistic mean electron density), non-neutral electron confinement in the modified Penning trap geometry chosen, and electron distribution functions which may be achieved.

The desired electron configuration would produce a spherical electron space charge potential, compatible with spherical ion focusing. Additionally, POPS operation requires that this ion well be harmonic, corresponding to a uniform electron density. Recently, it was shown[15] theoretically that such an electron configuration could be achieved in a hyperbolic Penning trap tuned to the spherical focussing condition previously demonstrated. It has also been proposed[16] (see subsequent discussion) that such a configuration may be approximated in a system which more easily allows higher applied voltages by removing the insulators far from the plasma volume. Unlike the hyperbolic case, this elongated system has no exact spherical symmetry. Thus, the desired electron configuration requires engineering the confinement fields to produce an approximate solution. The design of these fields in turn depends on the details of the electron distribution function. One needs to know this distribution relatively well to approximate the desired configuration.

On this basis, the PFX-I (Penning Fusion eXperiment-Ions) was proposed and constructed and has begun operation. PFX-I is a follow on to an electron-only, cryogenic, hyperbolic electron experiment, PFX.[17–19] In this paper, initial electron equilibrium and confinement results from PFX-I are reported. The following section reviews the theory of forming the desired electrostatic well. Constraints on the electron distribution are illustrated by assuming some relatively easily analyzed forms. Section III reviews the PFX-I experimental arrangement. Initial electron observations are reported in Sec. IV, while Sec. V contains a summary and conclusions.

II. ELECTRON EQUILIBRIUM AND ION WELL SOLUTIONS

Electron equilibrium in a trap of the Penning type is considered theoretically in this section. The geometry of interest [Fig. 1(a)] is similar to an electron Penning trap, but the end cathodes are removed axially from the trap volume. Electrons are transported from these cathodes along the applied magnetic field to the trap volume. In addition, the magnetic field may be made nonuniform by adding magnetically-soft iron for flux shaping. As in a more conventional Penning trap, radial electron confinement is provided by a strong axial magnetic field ($\geqslant 0.5$ T), which keeps electrons gyrating around the axial field lines. Axial electron confinement is provided by an electrostatic well of depth W_0 generated by the two negatively biased end cathodes, coaxial with the magnetic field, and a grounded anode, coaxial with the other two. The central anode is onion-shaped, and may be designed to induce a mirrorlike perturbation in the axial magnetic field such as that presented in Fig. 1(b) (which illustrates magnetic field lines).

A. Constraints on the electron distribution function

Before considering specific cases, a number of general features required of the electron distribution function F_e may be noted. These features follow from some very general goals related to ion confinement in the resulting electron space charge. Even before considering the detailed design shape (spherical) or gradient (harmonic), several general constraints may be derived. Assume that the system is axisymmetric and that the only constants of the motion are energy ε and canonical angular momentum, P_θ. Constraints on F_e may be derived from the requirements that they form a useful ion well.

Specifically, since it is desired that the ion well formed by electron space charge should be some reasonable fraction of the applied voltage V_0 (the higher the better), it follows that electrons must be nonthermal. The preferred electron energy distribution is a monoenergetic one, since this allows the single electron energy to be near the confinement limit ($W_0 = eV_0$). To see this, suppose the opposite; electrons are thermal with temperature T_e. Thermal electrons require both that the W_0 be large compared to $k_B T_e$ (k_B Boltzmann's constant), for electron confinement and that $k_B T_e$ be large compared to the ion well depth, for not too radical electron density variation within the ion well.[20] Thus, the electrons should be distributed in ε with a mean energy near W_0 with a relatively small energy spread.

A second constraint on the P_θ distribution may be seen from the requirement that an *axial* ion well be formed. For example, it can be shown that any Brillouin flow[21] electron distribution does not support an axial ion well. This arises from the transformation between ε and P_θ and velocity space. Thus, if $F_e = \delta(P_\theta) f(\varepsilon)$, the number density n is

$$n = \frac{2\pi}{m^2 R} \int dP_\theta \int d\varepsilon F_e = \frac{2\pi}{m^2 R} F\left(-e\Phi + \frac{e^2 A_\theta^2}{2m} \right), \quad (1)$$

where R is the cylindrical radius, e and m are the electron charge and mass, Φ is the electrostatic potential, A_θ is the azimuthal component of the vector potential, and F is the indefinite integral of the energy dependence function f. It may be seen from (1) that as $R \to 0$, the condition $F(-e\Phi) = 0$ determines $\Phi = \text{const.}$, so no electrostatic potential exists along $R = 0$ to form an axial ion well.

The above negative conclusion might be expected to hold, at least approximately, for any distribution which is strongly peaked near $P_\theta = 0$ and for which the P_θ and the ε

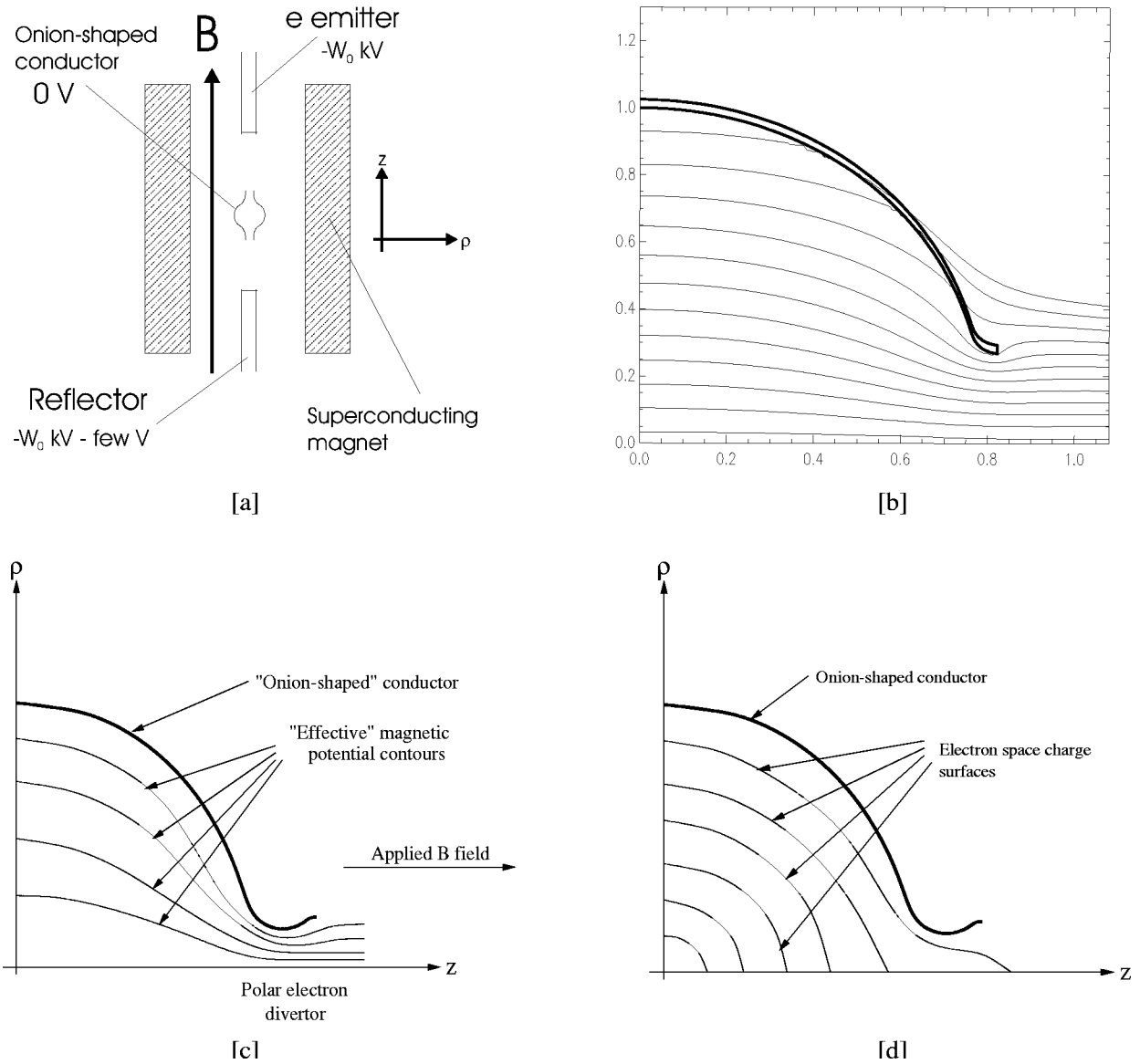

FIG. 1. Method for forming spherical ion well in modified Penning trap. (a) Trap schematic; (b) magnetic field lines (constant RA_θ); (c) effective magnetic potential; (d) self-consistent electrostatic contours.

variation are independent. One might well ask whether there are any examples of distributions for which an axial ion well exists. One such example is given next, where the case of a monoenergetic rigid rotor distribution is shown to give solutions with the desired properties.

B. Rigid rotor distribution

Consider now the specific case of a rigid-rotor distribution confined in a mirror geometry as shown in Fig. 1(b). The mirrorlike magnetic field provides both radial (cyclotron orbits) and axial (mirror effect) electron confinement within the conductor, except at the polar regions, where the electrons can leak out along the axis (although they are still confined by the axial magnetic field and the end electrodes). The magnetic field is shaped so that energetic electrons cannot reach the anode wall, thus avoiding electron losses.

A highly spherical confined electron cloud is desired for ion focusing. This in turn requires adequate design of the conductor shape and the strength of the magnetic field, corresponding to the particular steady-state electron distribution. For a *rigid rotor* distribution of electrons with rotation speed Ω_e, and for the ideal axial magnetic field [as depicted in Fig. 1(b), which is characterized by the single component of the vector potential A_θ], the electron distribution function can be expressed as $F_e = F_e(\varepsilon - \Omega_e P_\theta)$. By transformation to the rotating reference frame, the argument $\overline{\varepsilon} = \varepsilon - \Omega_e P_\theta$ (which can be regarded as the relative electron energy in the rotating frame) may be written as

$$\overline{\varepsilon} = \frac{m_e \overline{v_e}^2}{2} - e(\Phi + \Phi_{A,e}), \tag{2}$$

where m_e is the electron mass, $\overline{v_e}$ is the magnitude of the relative electron velocity in the rigid-rotor rotating frame, Φ is the electrostatic potential (nearly all due to the electrons space charge), and $\Phi_{A,e}$ is the effective magnetic potential for the electrons, given by

$$\Phi_{A,e} = -\Omega_e R A_\theta + \frac{m_e \Omega_e^2 R^2}{2}. \tag{3}$$

The effective magnetic potential $\Phi_{A,e}$ embodies the effect of the magnetic field on the electrons in the rotating reference frame. In an ideal electron system, $\Phi_{A,e}$ should be constant on the (nearly) spherical boundary of the onion-shaped conductor, and equal to the maximum electron energy (to prevent electrons from colliding against the conductor). Thus, the onion-shaped conductor acts as both a magnetic potential surface and the anode of the system. The approximate shape of the effective magnetic potential surfaces in this case is depicted in Fig. 1(c).

The actual shape of the electron space charge, Φ, is given by the self-consistent solution of the following Vlasov–Poisson system:

$$\nabla^2 \Phi = \frac{e}{\varepsilon_0} \int d\mathbf{v} F_e(\varepsilon - \Omega_e P_\theta) = \frac{e n_e(\Phi + \Phi_{A,e})}{\varepsilon_0}, \tag{4}$$

where e is the electron charge, n_e is the electron density. Clearly, Φ depends strongly on the actual functional form of the electron rigid-rotor distribution function F_e. Assuming the electron distribution is monoenergetic in the rotating reference frame, the corresponding electron space charge obtained with the self-consistent Vlasov–Poisson system posed in (4) is approximately harmonic within the onion-shaped conductor [Fig. 1(d)], and the electron density is constant within a volumetric-averaged error of 3%–5%.

The successful confinement of electrons as described above results in a uniform spherical electron cloud at the center of the onion-shaped conductor, with space charge potential given by

$$\Phi(r) = \frac{e n_e r^2}{6 \varepsilon_0}, \tag{5}$$

where r is the spherical radius. Equation (5) represents a harmonic well for the ions. The unneutralized space charge determines the maximum system size, as excessive electric field at the conductor's wall would result in electrical breakdown. Practical considerations limit the fusion cell radius to $\sim$1 cm, with electron densities of $10^{18}\,\mathrm{m}^{-3}$, and maximum electron space charge potential $\sim$300 kV. The actual potential in the system is smaller due to space charge neutralization by ions.

C. Experimental electron distribution

Even though the rigid-rotor distribution considered in the previous subsection offers a desirable electrostatic ion well, it is not known exactly how to engineer this distribution in a real system. Many nonideal factors affect the exact equilibrium electron distribution produced. Some of these are, electron–neutral collisions, electron–ion collisions, secondary electrons produced by impact ionization, and field errors, especially those near the turning points for axial electron motion. Because it is difficult to model all of these factors, the electron distribution realized experimentally is considered an empirical function, and the emphasis is currently being placed on measurement of the electron equilibrium under actual experimental conditions. Once the electron distribution is determined empirically, computer calculations of the sort carried out for the rigid-rotor distribution may be used to well approximate the desired spherical ion well.

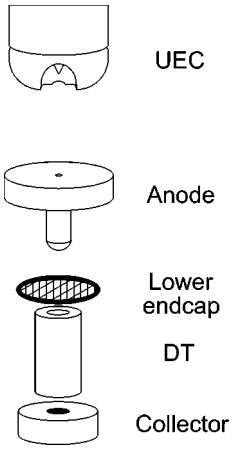

FIG. 2. Schematic of the trap showing the upper endcap (UEC), the anode, lower endcap, drift tube (DT), and collector. A cutout in the UEC reveals the tungsten emitter and beam exit hole. The drawing is not to scale.

III. THE PFX-I EXPERIMENT

As discussed in the previous section, applied voltages of the order of 100 kV are required. In order to increase the voltage standoff of our trap, we have modified the standard electron Penning trap geometry significantly. Chief among the modifications is the increased separation of the endcaps and the anode as well as the nonhyperbolic shape of the surfaces of these electrodes. A schematic diagram of the trap is shown in Fig. 2, and the trap is described in detail below.

In PFX-I the electron beam is produced by a tungsten hairpin filament located inside a stainless steel electrode, which serves as both the upper endcap (UEC) of the trap and the Wehnelt (grid) for the electron gun. This electrode is one of three electrical connections to the electron gun. All three connections are nominally at or near the trap high voltage, V_0 (negative). The filament leads are held at some small positive voltage, $V_b \sim 1$ V, with respect to the UEC. The emitting tip of the filament is located roughly 3 mm behind the front surface of the UEC and in the center of an approximately 4 mm diameter hole.

The UEC assembly operates as a conventional electron gun, and emission may be cut off by a sufficient positive bias of the filament with respect to the UEC, proportional to V_0. Above this cutoff emission into the trap ceases, and the beam can be turned on or off quickly ($\sim$80 μs) by setting V_b below or above this cutoff voltage. In this configuration, the potential as seen by the electrons across the plane of the hole in the UEC has a minimum (electrical potential maximum) at $R=0$, i.e., the filament location. Electrons reflected back by the lower endcap, as described below, are then able to escape axially only through some small cylindrical aperture centered at $R=0$.

The confinement region of PFX-I consists of a grounded anode, which is topologically a cylindrical cavity. Both elec-

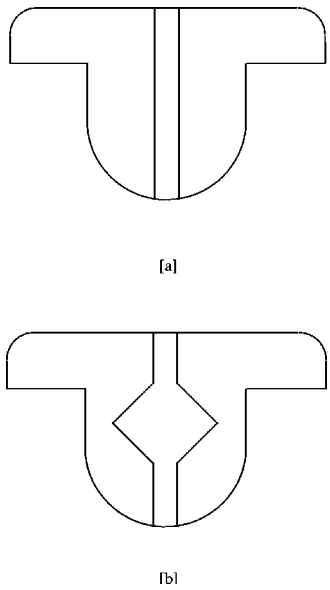

FIG. 3. Two anodes used in initial PFX-I operation. (a) Uniform cylindrical cavity; (b) uniform taper electrostatic shaping test cavity.

trostatic shaping (by choosing the section of the inner anode surface) and magnetic shaping (by introducing magnetically-soft iron flux shaping) may be used to achieve the desired electron density distribution. PFX-I has operated with two different anodes, and has not yet attempted to combine magnetic shaping with electron confinement. Electrostatic shaping has been studied by comparison of two simple anode shapes. A first stainless steel anode is approximately 18 mm thick with a 2 mm uniform diameter hole [Fig. 3(a)]. A second configuration, intended to investigate electrostatic shaping, replaces this cylindrical anode cavity with a diamond-shaped cavity, formed by two 90° cones meeting at the equator [Fig. 3(b)]. There is a 2 mm diameter entrance/exit hole at the apex of each cone. Electrical current to the grounded anode is monitored externally. The trap axis is aligned with the magnetic field axis by positioning the trap to minimize this current. Figure 4 contains a schematic of the electronic arrangement of the apparatus.

Below the lower surface of the anode a 60% transparent grid serves as the lower endcap or reflector. In high voltage operation, this reflector is allowed to ''float'' or is grounded through a very large resistance (>10 GΩ) and charges to near $-V_0$, so that electrons are reflected. For the low-voltage (<3 kV) operation reported here this electrode is maintained at a sufficiently negative voltage to reflect the electron beam and maintain axial confinement, but can be switched to ground potential with a variable time delay after halting electron emission from the filament. Trapped electrons then escape to a microchannel plate (MCP), which acts as a charge collector. The escaping electrons charge the collector negatively, generating a voltage pulse, which is monitored by an oscilloscope.

Between the lower endcap and the collector is a drift tube. The drift tube is maintained at a fixed potential throughout the trap operation thereby decreasing the amplitude of the capacitive component of the collector signal. The

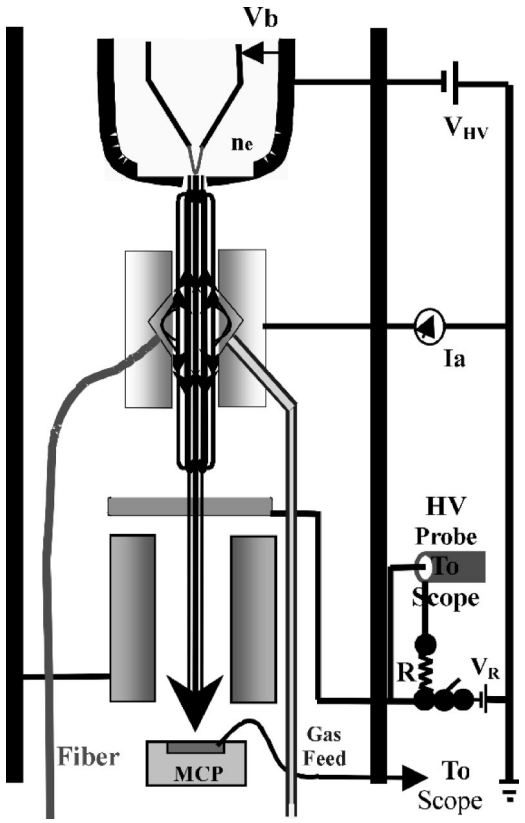

FIG. 4. Electrical schematic of the trap apparatus.

drift tube may be biased positively to facilitate electron transport to the collector.

The entire trap is contained within an ultrahigh vacuum system with a base pressure of several$\times 10^{-8}$ Torr maintained by a 50 ℓ/s ion pump. The vacuum system inserts into the room temperature bore of a superconducting magnet capable of producing fields up to 7 T, although for the experiments reported here the fields used were less than 1.5 T.

The high voltage for the upper endcap and electron emitter is provided by a supply capable of providing 100 kV. This supply is used to float an instrument rack, which contains the filament current and bias supplies and various current monitoring devices, to high voltage. The rack is powered by an isolation transformer and its instruments are controlled via an optical link. In this way, the electron source may be flexibly programmed and both the applied voltage and the emission current (by modulation of the filament to UEC bias) may be varied at up to rf frequencies.

In addition to the destructive measurement technique described above, the electron density and space-charge electric field strength within the trap volume, n_e, can be measured optically. If atoms or molecules of some species, M, are excited by the process $e^- + M \rightarrow M^* + e^-$, then the rate per unit volume at which particles are excited is proportional to the electron density. The photon emission rate per unit volume is equal to this excitation rate provided that the lifetime of the excited state is short compared to the residence time of the particles in the trap. For electric dipole transitions this is always the case. Hence, the rate at which photons are produced is $\rho = n_0 \int d\mathbf{v} n_e F_e(v) v \sigma(v)$, per unit volume. Here n_0

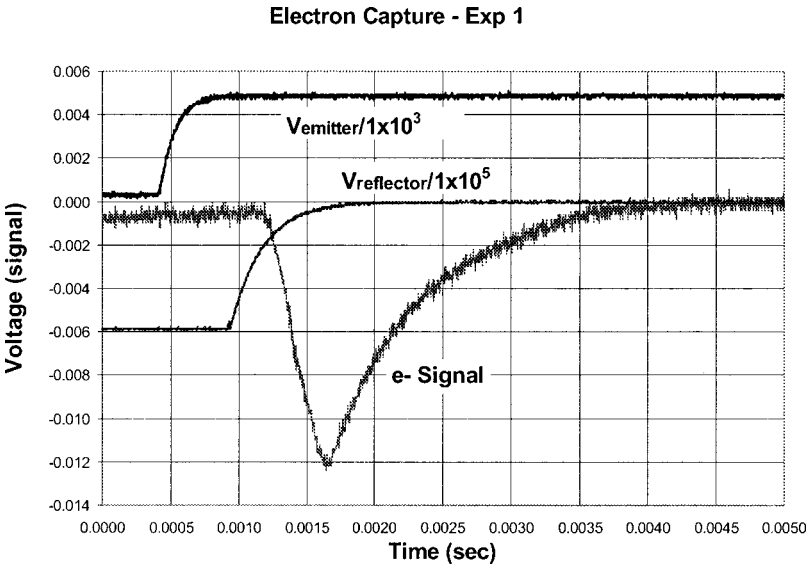

FIG. 5. Timing sequence for destructive electron inventory measurement. Upper trace is filament to UEC voltage vs time. Lower trace is reflector voltage to ground. Middle trace is collected electron current, whose integral is proportional to the trap inventory at the time of the reflector voltage drop.

is the (uniform) neutral density, v and $F_e(v)$ are the velocity and the (assumed isotropic) distribution function of the electrons, respectively, and $\sigma(v)$ is the energy-dependent cross section for the excitation process. The electron density can then be calculated from the measured photon flux from the trap.

Neutral gas is introduced into the trap anode volume through a long 1 mm diameter tube. Photons are collected by a 200 μm diameter optical fiber with an effective acceptance angle of 8° located approximately 1 cm away from the center of the trap volume. The light is wavelength analyzed by a half-meter monochromator and counted by a chilled photomultiplier tube. The expected signal, then, is $S=\kappa\rho$, where the constant κ depends on the volume of the plasma viewed by the fiber, the solid angle subtended by the fiber and its transmissivity, and the efficiency of the photomultiplier tube and monochromator. This calibration constant and optical results are discussed in the next Section, where initial PFX-I observations are reported and analyzed.

IV. ELECTRON EQUILIBRIUM AND CONFINEMENT IN PFX-I

A. Operation and data

PFX-I has been operated with electrons at high vacuum conditions or with neutral gas pressures up to a few 10^{-4} Torr introduced through the gas system.

Electron inventory in PFX-I has been measured as a function of applied voltage V_0, (uniform) magnetic field B, delay time t, and neutral pressure P_0. Two diagnostics have been used to study the electron inventory and volumetric density. A destructive measurement of inventory is obtained by ''dumping'' the electron cloud after a sustainment period during which steady state has been achieved. This sequence was briefly described in the previous section, and may be understood by reference to Figs. 4 and 5.

A steady state is established for a specified V_0 and B by biasing the filament negative relative to the UEC (V_b) initiate electron emission, while the reflector is biased sufficiently more negatively than V_0 to reflect essentially all electron current back into the trap. After ''filling'' the trap for a period of several seconds, steady state parameters including base pressure (from which the pressure in the anode can be calibrated) and electrode currents, including anode current I_A are monitored.

To determine the electron inventory $N(t)$, emission is switched off by rapidly changing V_b to a large enough positive value (upper trace of Fig. 5). A programmed delay time t elapses after which the reflector is ''dumped'' to ground (lower trace of Fig. 5), allowing a large fraction (60% transparency) to pass down through the drift tube to the collector, producing a voltage pulse from the electron charge (middle trace of Fig. 5). Integration of the electron signal when electrons are loaded into the trap determines the inventory at time $t>t_{\min}$, where the minimum interrogation time is set by the control system and response of the various switches.

Initial data were obtained with $t_{\min}=30$ ms with the cylindrical anode over a range of V_0 and B.[20] These data show that both $N(t_{\min})$ (Ref. 20) and I_A increase linearly with V_0 at fixed B. Recently, similar data have been obtained with the shaped cavity anode and with $t_{\min}$ reduced to 0.2 ms by improvements in the control system. Figure 6 shows $N(t)$ obtained with $V_0=400$ V, $B=1$ T, and with two different anode pressures. The upper curve of Fig. 6 shows $N(t)$ for the base pressure conditions, while the lower curve shows a similar history for a case when the lowest gas source measurable was introduced (the gas presence was monitored by increasing I_A). An exponential fit to both curves shows a confinement time (based on exponential decay) of 0.91 (0.70) ms for these two conditions. As discussed below, this change of confinement is consistent with the neutral pressure in the anode.

A second measurement of electron density is provided by the optical diagnostic. Initial measurements in PFX-I have been conducted using the 391.4 nm light of the nitrogen molecular ion, N_2^+. A typical emission spectrum of nitrogen is shown in Fig. 7. An estimate of the absolute calibration factor κ of the previous section was used to estimate n_e.

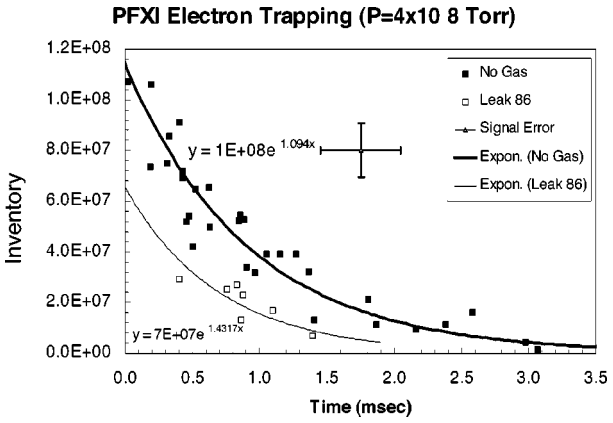

FIG. 6. Electron inventory vs delay time t for two neutral pressure conditions at $V_0=400$ V, $B=1$ T with shaped cavity anode.

This spectrum was taken with a N_2 anode pressure of approximately 1.2×10^{-5} Torr, and the resulting peak signal of 270 s^{-1} at 391.4 nm yields an estimated electron density of 10^7 cm^{-3}. However, there are two sources of uncertainty which complicate the analysis. First, photons not emitted into the acceptance angle of the fiber may be reflected by the stainless steel wall of the anode and enter the fiber after one or more reflections. Accounting for this effect is difficult but would tend to lower the calculated electron density.

A more serious complication arises from lack of knowledge of the electron velocity distribution. Although a beam with an energy spread of a few electron volts is injected into the trap, the actual energy distribution of the electrons within the trap may be quite different from this beam distribution due to thermalization of the beam electrons and production of secondary electrons by collisions with the neutral background gas. As the cross section for the process of interest is strongly energy dependent (see, for example, Kieffer and Dunn[22]), the photon production rate is very sensitive to this distribution function. Without a measurement of the trapped electron energy distribution, it is impossible to estimate the extent of this effect.

B. Interpretation and scaling

A simple view of the initial PFX-I data shows several features of the trap operation. First, electron confinement is strongly dependent on neutral pressure. This is evident by the degradation of confinement shown in Fig. 6, where the anode pressure is changed roughly by 20% (as evidenced by the change of the anode current from 250 nA to 300 nA when gas was introduced). At higher neutral pressures, no electron signal is detected by dumping the trap, either because the inventory is so much reduced or because the confinement time becomes much shorter that $t_{\min}$. Further, the spectroscopic estimate of electron density is two orders of magnitude lower than that estimated from the inventory (using a trap volume of 0.2 cm^3), which may be consistent with the two orders of magnitude increase in the neutral pressure. Thus, it appears that confinement time decreases with neutral pressure, and that, confinement time is determined by neutral pressure, down to the lowest base pressures achievable with the present vacuum system.

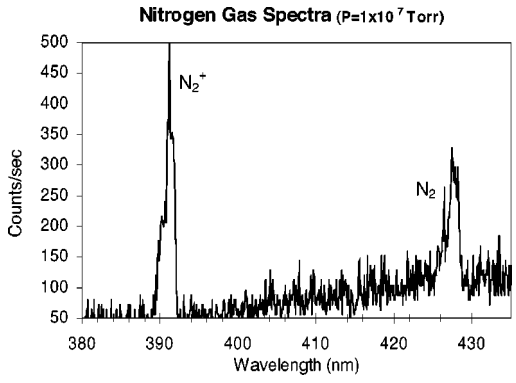

FIG. 7. Emission spectrum for the N_2 trap fill.

TABLE I. Analysis of confinement scaling vs magnetic field B. N_{30} is inventory 30 ms, I_A anode current. N_0 and τ are inferred initial inventory and confinement time.

B (T)	$N_{30}(10^8)$	I_A (nA)	$N_0(10^8)$	τ_0 (ms)
0.38	0.76	54	28.0	8.32
0.76	2.79	18.3	18.3	16.0
1.14	4.11	16.5	19.7	19.1

Secondly, the linear variation of both anode current and inventory with applied voltage indicates that the confinement time τ is independent of V_0. An analysis of confinement variation with B shows that τ increases with B. For this, it is first noted that the linear variation of inventory with V_0 indicates that the trap is filling to the space charge limit.[20] That is, the electron profile density will increase until the self space charge is equal to the applied voltage. Also consistent with this is the decrease of emitted current (equal to the anode current I_A) by several orders of magnitude when the reflector is biased sufficiently negative. If the electron profile is independent of B, the electron inventory should be also. The earliest time inventory[20] is then used to extract a confinement time as follows.

It is assumed that N decays as $N(t)=N_0\exp(-t/\tau)$. Then, using $I_A=eN_0/\tau$ and $N(t_{\min})=N_0\exp(-t_{\min}/\tau)$, the two parameters N_0 and τ are determined from the two observed quantities I_A and $N(t_{\min})$. The results, shown in Table I, indicate that N_0 is roughly independent of B (maximum deviation occurs at lowest B where extrapolation is largest) and that τ increases with B, roughly linearly for small B, and more slowly (possibly saturating) for larger B.

In comparison to these results for the cylindrical anode [Fig. 3(a)], τ is significantly decreased for the cavity anode [Fig. 3(b)]. In contrast to $\tau=15$ ms from Table I, electron inventory history for the cavity anode (Fig. 6) shows $\tau\approx1$ ms. It is not presently known whether this decrease is associated with increased neutral pressure or with some other effect of the anode shape. For example, if ions are trapped within the cavity anode, electron collisions with these ions might lead to more rapid cross-field transport.

The spectroscopic measurement of n_e is limited by uncertainties noted previously. The estimate of the electron

density given above is, at best, an order of magnitude calculation. The uncertainty stems from the dependence of this technique on measuring the absolute photon production rate. Although much can be done to improve the measurement by reducing the reflectivity of the anode and determining the energy distribution of the trapped electrons, a measurement technique which is independent of the photon production rate is essential. We are implementing an optical technique based on Stark splitting of hydrogen emission lines in a strong electric field.[23] In this case, the electric field is provided by the space charge of electron plasma, and the magnitude of the splitting depends on the electron density. The photon production rate is only important in determining the signal to noise ratio of the diagnostic. Estimated splittings range from 0.1 nm to 1.5 nm as the electron density increases from $5\times10^{9}\,\mathrm{cm}^{-3}$ to $1\times10^{12}\,\mathrm{cm}^{-3}$. To reach such densities will require operating the trap at the space-charge limit at voltages up to 100 kV.[18]

V. SUMMARY AND CONCLUSIONS

Theoretical advances in techniques for ion focussing which can produce high thermonuclear Q have shown that forming the desired electron configuration in a trap of the Penning type may lead to a desirable fusion system by combining ion focusing with non-neutral electron confinement. The desired electron configuration is a nearly uniform density, spherical system. Such a configuration can be approximated by a combination of electrostatic shaping and magnetic shaping, if the correct electron distribution can be produced in a quiescent electron plasma with satisfactory (near nonneutral) confinement.

A combined trap, PFX-I (Penning Fusion eXperiment-Ions) has been constructed and has begun electron operation to investigate these possibilities. Initial operation has focussed on low voltage (<2 kV) conditions for which direct electrical diagnostics are feasible. A noninvasive optical diagnostic has also been realized by spectroscopic analysis of electron impact induced fluorescence of injected low-pressure neutral gas. Calibration of direct electrical measurements and optical measurements will allow us to remove high voltage limiting wiring and operate the system at full voltage.

Initial results show electron trapping consistent with filling the trap to the space charge limit, in that the electron inventory is proportional to applied voltage and (roughly) independent of magnetic field. Confinement times are of order 1 to a few ms, long for a 1 mm radius cylindrical system, but much shorter than might be expected from cross-field transport of a non-neutral plasma. Furthermore, confinement seems to be determined by neutral pressure. The combination of these two observations poses a theoretical question, in that confinement times are of order of the electron–neutral collision time, meaning that an electron must be lost in a single collision, while the electrons are strongly magnetized, so that the gyroradius is much smaller than the system radius. Theoretical possibilities being investigated include combination of neutral collisions with field error induced orbit drifts and collisions with trapped ions.

The preliminary work reported here will be extended during the next experimental period. In addition to more complete parameter scans of confinement scaling of electrons, the spectroscopic system will be improved by an improved calibration and by operation at higher applied voltages, where Stark splitting is expected. Additional electrostatic shaping and magnetic shaping will be designed and applied as the electron distribution is better understood theoretically, with the goal of producing an electrostatic well for trapping ions during the next period. Finally, diagnostics, including MCP ion measurements, will be developed to observe ions trapped electrostatically within the anode volume.

ACKNOWLEDGMENTS

This work was supported by the U.S. Department of Energy, Office of Fusion Energy Science. The authors acknowledge the continuing assistance and advice of M. H. Holzscheiter, L. S. Schrank, and F. L. Ribe of Los Alamos.

[1] R. L. Hirsch, J. Appl. Phys. **38**, 4522 (1967).
[2] R. W. Bussard, Fusion Technol. **19**, 273 (1991).
[3] N. A. Krall, Fusion Technol. **22**, 42 (1992).
[4] W. M. Nevins, Phys. Plasmas **2**, 3804 (1995).
[5] T. N. Tiouririne and D. C. Barnes, Bull. Am. Phys. Soc. **40**, 1665 (1995).
[6] Y. Gu and G. H. Miley, ''Experimental study of potential structure in spherical IEC fusion device,'' IEEE Trans. Plasma Sci. (to be published).
[7] K. Yoshikawa *et al.*, ''Real time measurements of strongly localized potential profile through Stark effects in the central core region of an inertial-electrostatic confinement fusion device,'' Proceedings of the 18th IEEE/NPSS Symposium on Fusion Engineering, Albuquerque, NM, October 25–29, 1999 (IEEE Operations Center, Piscataway, 2000) (to be published).
[8] L. Chacon, D. C. Barnes, D. A. Knoll, and G. H. Miley, J. Comput. Phys. **157**, 618 (2000).
[9] L. Chacon, D. C. Barnes, D. A. Knoll, and G. H. Miley, J. Comput. Phys. **157**, 654 (2000).
[10] L. Chacon, D. C. Barnes, D. A. Knoll, and G. H. Miley, ''A bounce-averaged Fokker–Planck code to model ion physics in Penning inertial electrostatic confinement fusion systems,'' Comput. Phys. Commun. (submitted).
[11] L. Chacon, D. C. Barnes, D. A. Knoll, and G. H. Miley, ''Energy gain calculations in spherical inertial electrostatic Penning fusion systems using a bounce-averaged Fokker–Planck model,'' Phys. Plasmas (submitted).
[12] D. C. Barnes and R. A. Nebel, Phys. Plasmas **5**, 2498 (1998).
[13] R. A. Nebel and D. C. Barnes, Fusion Technol. **34**, 28 (1998).
[14] R. A. Nebel and J. M. Finn, Phys. Plasmas **7**, 839 (2000).
[15] D. C. Barnes, Phys. Plasmas **6**, 4472 (1999).
[16] M. M. Schauer, ''PFX-I (Penning Fusion eXperiment-Ions)'' proposal submitted to Office of Fusion Energy Sciences, Office of Energy Research, U.S. Department of Energy, in response to Program Announcement LAB-97-08, ''Innovations in Fusion Energy Confinement Systems'' See AIP Document No. EPAPS E-PHPAEN-7-935005 for PFX-I proposal. EPAPS document files may be retrieved free of charge from our FTP server (http://www.aip.org/pubservs/epaps.html) or from ftp.aip.org in the directory /epaps/. For further information, e-mail: paps@aip.org or fax: 631-576-2223.
[17] T. B. Mitchell, M. M. Schauer, and D. C. Barnes, Phys. Rev. Lett. **78**, 58 (1997).
[18] D. C. Barnes, T. B. Mitchell, and M. M. Schauer, Phys. Plasmas **4**, 1745 (1997).
[19] M. M. Schauer, T. B. Mitchell, M. H. Holzscheiter, and D. C. Barnes, Rev. Sci. Instrum. **68**, 3340 (1997).
[20] M. M. Schauer, K. R. Umstadter, and D. C. Barnes, *The Penning Fusion*

Experiment: Ions, in *Non-Neutral Plasma Physics III*, edited by J. J. Bollinger, R. L. Spencer, and R. C. Davidson, AIP Conf. Proc. 498 American Institute of Physics (Melville, NY, 1999).
[21]L. Brillouin, Phys. Rev. **67**, 260 (1945); M. Reiser, *Theory and Design of Charged Particle Beams* (Wiley, New York, 1994), p. 317.
[22]L. J. Kieffer and G. H. Dunn, Rev. Mod. Phys. **38**, 1 (1966).
[23]H. A. Bethe and E. E. Salpeter, *Quantum Mechanics of One- and Two-Electron Atoms* (Springer-Verlag, New York, 1957), pp. 228–232.